PAPER • OPEN ACCESS

Super-long bridges with floating towers: the role of multi-box decks and Hardware-In-the-Loop technology for wind tunnel tests

To cite this article: A Zasso *et al* 2017 *IOP Conf. Ser.: Mater. Sci. Eng.* **276** 012008

View the article online for updates and enhancements.

Related content

- Research on Modelling of Aviation Piston Engine for the Hardware-in-the-loop Simulation
  Bing Yu, Wenjun Shu and Wenchao Bian

- Industrial wind tunnels
  J A Balchin

- Triboelectret-based aeroelastic flutter energy harvesters
  Matthias Perez, Sebastien Boisseau, Matthias Geisler et al.

IOP ebooks™

Bringing you innovative digital publishing with leading voices to create your essential collection of books in STEM research.

Start exploring the collection - download the first chapter of every title for free.

Super-long bridges with floating towers: the role of multi-box decks and Hardware-In-the-Loop technology for wind tunnel tests

A Zasso, T Argentini, I Bayati, M Belloli, D Rocchi

Politecnico di Milano: Department of Mechanical Engineering, Milano, Italy

Contact author: tommaso.argentini@polimi.it

Abstract. The super long fjord crossings in E39 Norwegian project pose new challenges to long span bridge design and construction technology. Proposed solutions should consider the adoption of bridge deck with super long spans or floating solutions for at least one of the towers, due to the relevant fjord depth. At the same time, the exposed fjord environment, possibly facing the open ocean, calls for higher aerodynamic stability performances. In relation to this scenario, the present paper addresses two topics: 1) the aerodynamic advantages of multi-box deck sections in terms of aeroelastic stability, and 2) an experimental setup in a wind tunnel able to simulate the aeroelastic bridge response including the wave forcing on the floating.

1. Introduction

The super long fjord crossings in E39 Norwegian project pose new challenges to large span bridge design and construction technology. Proposed solutions should consider the adoption of super long spans for the deck or floating solutions for at least one of the towers, due to the relevant fjord depth. At the same time, the exposed fjord environment, possibly facing the open ocean, calls for higher aerodynamic stability performances, compared to the existing long-span bridges further inland.

The choice of the multi-box deck section concept has reached nowadays a proven technological development and reliability, offering its superior aerodynamic performances as possible key solution for a high aerodynamic stability request [1][2][3]. At the same time the closed box girder streamlined solution with higher aerodynamic performances is also offering the great advantage of limited mass of the deck per unit length, playing therefore a key role in case of floating tower solution. However, multi-box decks may show complex vortex shedding excitation phenomena and they should be thoroughly studied in wind tunnel [4][5][6].

Assessment of a considered suspension bridge solution with one or two towers on a floating support is posing non-trivial challenges in terms of experimental validation of the numerically simulated structure dynamics, based on hybrid codes accounting both for the aero- and the hydro-dynamic loads effect. The new technology of Hardware-In-the-Loop (HIL) testing recently developed at POLIMI in the field of floating offshore wind turbines is proposed as a reliable tool for the experimental validation of the complex numerical approach. A 6 degree of freedom platform driven by linear actuators is available at POLIMI at the purpose of simulating the motion of the floater due to the combined action of the hydrodynamic loads on the floater (numerically simulated in real time) and of the aerodynamic and inertial loads transmitted by the tower (measured by a 6 components dynamometer at the tower-

platform interface). The opportunities offered by the mentioned HIL technology are discussed with reference to a possible wind tunnel test experiment on a bridge aeroelastic model focused on the validation of the numerical hybrid tools needed for the floating bridge solution assessment.

2. The aero-hydro-elastic problem

Adopting the modal approach, the dynamics of a bridge can be written as:

$$\left[M_s^* \right]\underline{\ddot{q}} + \left[C_s^* \right]\underline{\dot{q}} + \left[K_s^* \right]\underline{q} = \left[\Phi \right]^T \underline{F}_{aero} + \left[\Phi \right]^T \underline{F}_{hydro} \tag{1}$$

where $\underline{q}$ is the vector of the modal coordinates; $\left[\Phi \right]$ the mode shape matrix, $\left[M_s^* \right]$, $\left[C_s^* \right]$ and $\left[K_s^* \right]$ are the structural inertial, damping, and stiffness modal matrices of the system; $\underline{F}_{aero}$ the external aerodynamic forces that depends on the motion of the deck and on the incoming wind velocity; $\underline{F}_{hydro}$ the external hydrodynamic forces acting on the floating structure, if present. Linearized and non-linear approaches differ in the modelling of both $\underline{F}_{aero}$ and $\underline{F}_{hydro}$.

2.1. The aeroelastic forces

The simulation framework for aeroelastic analyses of long-span bridges is rather well established, and it consists of the following points [7][8][9]:

- The bridge structural dynamics is represented by means of a modal approach, starting from a FEM of the structure.
- The deck is divided into several sections to which aerodynamic forces are applied. Each section, from an aerodynamic point of view, is independent from the other (sectional approach). Cables and towers may be analysed in the same way.
- For each deck section, the turbulent wind field is simulated starting from its stochastic characteristics (e.g. PSD, spatial coherence, turbulence intensity, integral length scale, etc.).
- The dynamic response of the bridge is computed, applying the aerodynamic forces to the deck sections and to other components. The aerodynamic forces depend on the deck state (position and velocity) and on the incoming turbulence.

The standard approach for buffeting response is based on a linearized model of the fluid-structure interaction around a steady configuration of the bridge, which depends on the mean wind speed field. The external aerodynamic forces ($\underline{F}_{aero}$) are computed as the sum of three different effects, namely:

$$\underline{F}_{aero} = \underline{F}_{ST} + \underline{F}_{se} + \underline{F}_{buff} \tag{2}$$

where $\underline{F}_{ST}$ are the stationary aerodynamic forces, $\underline{F}_{se}$ the self-excited, and $\underline{F}_{buff}$ the buffeting forces.

The steady aerodynamic drag, lift and moment forces acting on each deck section are defined through the steady coefficients as a function of the angle of attack:

$$\underline{F}_{ST} = \frac{1}{2}\rho V^2 B \begin{bmatrix} C_D \\ C_L \\ BC_M \end{bmatrix} \tag{3}$$

where B is the deck chord, V the mean wind velocity, and ρ the air density.

The self-excited unsteady aerodynamic terms of drag, lift and moment acting on each deck section (D , L , and M) are modeled using the flutter derivatives coefficients, measured with dedicated forced motion tests on rigid sectional model. The self-excited forces acting on the generic j-th section are defined as:

$$\begin{bmatrix} D_j \\ L_j \\ M_j \end{bmatrix}_{aero} = \begin{bmatrix} m^*_{aero,j} \end{bmatrix} \begin{Bmatrix} \ddot{y}_j \\ \ddot{z}_j \\ \ddot{\theta}_j \end{Bmatrix} + \begin{bmatrix} c^*_{aero,j} \end{bmatrix} \begin{Bmatrix} \dot{y}_j \\ \dot{z}_j \\ \dot{\theta}_j \end{Bmatrix} + \begin{bmatrix} k^*_{aero,j} \end{bmatrix} \begin{Bmatrix} y_j \\ z_j \\ \theta_j \end{Bmatrix} \tag{4}$$

where y_j, z_j and θ_j are respectively the lateral, vertical and torsional displacements of the j-th section, $\begin{bmatrix} m^*_{aero,j} \end{bmatrix}$, $\begin{bmatrix} c^*_{aero,j} \end{bmatrix}$ and $\begin{bmatrix} k^*_{aero,j} \end{bmatrix}$ are the aerodynamic matrices related to the j-th section, expressed as a function of the 18 flutter derivatives coefficients a^*_i, h^*_i and p^*_i with $i = \{1:6\}$.

a^*_i, h^*_i and p^*_i are proportional to the slopes of the static coefficients ($K_L = dC_L / d\alpha$; $K_M = dC_M / d\alpha$) and they are function both of the reduced velocity ($V^* = V / (fB)$, being f the motion frequency), and of the mean angle of attack.

Buffeting forces are due to the incoming turbulent wind. They are defined through the so-called aerodynamic admittance functions as:

$$\begin{bmatrix} D_j \\ L_j \\ M_j \end{bmatrix}_{buff} = \frac{1}{2}\rho V^2 B \begin{bmatrix} \chi_{D-u}\left(V^*,\alpha\right) & \chi_{D-w}\left(V^*,\alpha\right) \\ \chi_{L-u}\left(V^*,\alpha\right) & \chi_{L-w}\left(V^*,\alpha\right) \\ B\chi_{M-u}\left(V^*,\alpha\right) & B\chi_{M-w}\left(V^*,\alpha\right) \end{bmatrix} \begin{Bmatrix} \dfrac{u}{V} \\ \dfrac{w}{V} \end{Bmatrix} \tag{5}$$

where χ are the 6 aerodynamic admittance functions (asymptotic to quasi-steady values at large V*), proportional to the slopes of the static coefficients (dependent upon both of the reduced velocity and of the angle of attack α), while u and w are the turbulent horizontal and vertical components of the turbulent wind field. Admittance functions can be measured with dedicated wind tunnel tests using an active turbulence generator.

2.2. The hydrodynamic forces
Collecting the independent coordinates of motion of the floating towers in the x vector, the equations of motion of the global system can be written as

$$\underline{F}_{hydro} = -[A_\infty]\underline{\ddot{x}} - [R_s]\underline{\dot{x}} - [K_s]\underline{x} + \underline{F}_{rad} + \underline{F}_{visc} + \underline{F}_{moor} + \underline{F}^{(1)}_{diff} + \underline{F}^{(2)}_{diff} \tag{6}$$

where [A∞] is the wave frequency-independent or "infinite frequency" hydrodynamic added mass matrix due to the radiation of the semisubmersible platform [10], given as output by the panel code WAMIT, [Rs] a diagonal viscous linear damping matrix added to tune the numerical model compared to the results from free decay tests in the ocean basin [10] and [Ks] is the system stiffness matrix containing both the terms related to the hydrostatic as well as gravitation restoring computed with respect to the Sea Water Level (SWL), upon which the x axis lays. The contributions to $\underline{F}_{hydro}$ are summarized in the following paragraphs.

2.2.1. Radiation forces $\underline{F}$rad:
The radiation force partially accounted for by the term [A∞] in Equation 6 is also due to a convolution term (Equation 7) between the platform velocity and the retardation matrix [K(t)] (impulse response), describing the dissipation of energy of the platform motion due to the radiated waves generated by the platform itself. The matrix [K(t)] can be expressed in the wave frequency domain [K(ω)], as in Equation 10 as a function of the frequency dependent added mass and damping matrices [A(ω)] and [B(ω)] computed with the inviscid and irrotational panel codes such as, WAMIT.

$$\underline{F}_{rad} = \underline{\mu}(t) = \int_0^t K(t-\tau)\underline{\dot{x}}(\tau)d\tau \tag{7}$$

$$\begin{cases} \dot{\underline{q}}_r = [A_r]\underline{q}_r - [B_r]\dot{\underline{x}} \\ \hat{\underline{\mu}} = [C_r]\underline{q}_r \end{cases} \tag{8}$$

$$\underline{F}_{rad} = \underline{\mu}(t) \approx \hat{\underline{\mu}}(t) \tag{9}$$

$$[K(\omega)] = [B(\omega)] + j\omega([A(\omega)] - [A_\infty]) \tag{10}$$

Due the time-consuming computation of a convolution term for control or real-time application like the one presented, the matrix $[K(\omega)]$ was identified in the frequency domain [12] by means of another equivalent matrix $[\hat{K}(\omega)]$ leading to the corresponding memory effect term $\hat{\mu}$ m through a state space approximation, Equation 8-10, more effectively implemented in the HIL control, Figure 7.

2.2.2. Viscous forces F_{visc}

The viscous forces considered are due to the Morison's contribution derived by the integration along the possible platform's columns of the drag forces depending quadratically on the relative velocities v_{rel} between the platform and the wave particles, either along tangential t or axial ax direction by the drag coefficients C_d and C_{ax}, respectively

$$F_t(t) = \int_z \frac{1}{2} C_d D_z |v_{rel,t}| v_{rel,t} dz \tag{11}$$

$$F_{ax}(t) = \int_z \frac{1}{2} C_{ax} \pi \frac{D_z^2}{4 L_z} |v_{rel,ax}| v_{rel,ax} dz \tag{12}$$

The forces are collected into the F_{visc} of the Equation 6 with a simple 2D rotation in the z-x plane. The particle velocities (along x and z directions) accounted in V_{rel}, along with the platform's velocities, are computed in the real time model, according the linear Airy theory of wave kinematics. Moreover, the Wheeler wave stretching is implemented along with the linear wave kinematics, to model also the contribution above the free surface

2.2.3. First order diffraction forces $F^{(1)}_{diff}$.

The first-order wave excitation loads (diffraction) were obtained based on complex frequency dependent wave exciting force vector $X(\omega_k)$ computed by WAMIT (i.e. output file *.3) and for a unitary wave amplitude h, for each i-th degree of freedom, under the assumption of a linear wave surface approximation. Therefore, the linear diffraction force is computed, as in Eq. 13, considering the random phased wave amplitudes spectrum A_k, consistent with a JONSWAP spectrum for a given sea state.

$$F^{(1)}_{diff,i} = \Re \left\{ \sum_{k=1}^{N} A_k X_i(\omega_k) e^{j\omega_k t} \right\} \tag{13}$$

2.2.4. Second order diffraction forces $F^{(2)}_{diff}$

The second-order difference-frequency potential-flow terms are also taken into account. Similarly to $F_{(1)}$ diff, "sum" and "difference" frequency normalized complex force matrices, $X^+(\omega_k ; \omega_l)$ and $X(\omega_k;\omega_l)$, also known as Quadratic Transfer Functions QTF, are taken from WAMIT's output (i.e. .12s/.12d file), which is the state-of-the-art in 3D panel code for offshore hydrodynamics, as function of each combination of incoming wave frequencies ω_k and ω_l. More specifically, full QTF loads taken as reference account for quadratic interaction of first order quantities plus second-order potential derived by the direct method (the formulation of the Boundary Integral Equation - BIE involves integrating the potential itself over the surface). However, the second order diffraction forces, sum (+) or difference (-) frequency forces, Equation 14, are taken into consideration for their importance in the modelling of floating systems, since they excite the rigid natural frequencies typically in the low frequency spectrum range   (-) for semisubmersible and spar buoys platforms, as assessed in [13], or in the high frequency range (+) for Tension Leg Platforms (+). Analogously to Equation 8, this contribution can be written as

$$F_{diff,i}^{(2)} = \Re\left\{ \sum_{k=1}^{N} \sum_{l=1}^{N} A_k A_l^* X_i^{+/-}(\omega_k, \omega_l) e^{j(\omega_k - \omega_l)t} \right\} \tag{14}$$

where the complex vector A_l is the same as A_k but transposed and evaluated at the l-th frequency of the JONSWAP spectrum. Also, a second-order correction to the linear sea surface elevation h is applied to take into account low-frequency range non-linearities (difference) of A_i, [14].

2.3. Validation of the hydrodynamic model
The hydrodynamic model, which is implemented on the real-time HIL controller, is designed to be fast but comprehensive of the complex hydrodynamics of a floating system. For this reason, a preliminary code-to-code comparison is carried against a fully non-linear hydro-elastic code (e.g. NREL/HydroDyn). More specifically, free decays along the principal degrees-of-freedom being investigated, the response of the platform due to regular waves (i.e. Response Amplitude Operators, RAO) and irregular random sea, are compared against the reference code. These tests are carried out considering no-wind conditions. On top of this, the corresponding tests might have been carried out also in ocean basin, so that the fine tuning of the model (e.g. linear and quadratic added damping) can be finalized relying also on the experimental data. An example of this procedure can be found in [13] where a two degrees of freedom (2-dof) HIL system (surge and pitch) has been developed for simulating the motion of a 5MW floating wind turbine, showing excellent agreement of the hydrodynamic modelling approach compared either with the reference numerical code and the ocean basin data.

2.4. Aeroelastic stability improvement
The aerodynamic performances of streamlined multi box decks have been extensively studied for many super long span bridges (e.g. [1][2][3]) . Figure 1 shows a comparison of a single-box deck (Storebaelt Bridge), a two-box deck (Stonecutters bridge) and a 3-box deck (Messina bridge).
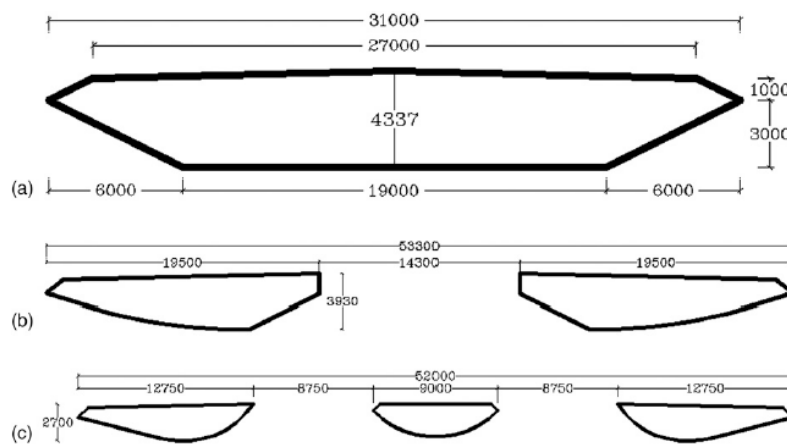

Figure 1. Cross-sections of decks: a) Storebaelt Bridge, b) Stonecutters bridge, c) Messina bridge (from [15])

From an aerodynamic point of view, the multi-box decks have better performances in terms of stability and buffeting responses, because of their smaller aerodynamic coefficients. As an example, Table 1 shows the derivatives of the lift and moment coefficients (K_L and K_M) for the 3 previous sections, having considered for each section its own chord width in the definition of the coefficients. If one compares the effects of these three different aerodynamic behaviors on the same bridge (Storebeaelt) with a very simplified approach, keeping unchanged the structural parameters and changing only the values of K_L and K_M, the results for stability shown in Figure 2 are obtained: predicted flutter speed goes from 70 to 120 to 240 m/s.

2.5. Issues in multi-box sections

However, multi-box section must be carefully investigated in wind tunnel for complex vortex shedding phenomena and subsequent vortex-induced vibration, and for the strong non-linear effects that may be relevant.

For vortex shedding, the presence of multiple boxes often introduces multiple lock-in ranges. As an example, the VIVs amplitude for the Messina bridge, which is a 3-box deck, are reported as a function of the reduced wind speed in Figure 3 (see [4]): two lock-in regions are present.

As far as the nonlinear effects are concerned, the most relevant characteristics can be found in the double nonlinear dependence of the aerodynamic forces on the amplitude of the angle of attack and on the reduced velocity (e.g. see Figure 4, where it is shown the nonlinear dependence of the lift coefficient upon the amplitude on the angle of attack and reduced velocity during forced motion tests). This nonlinearity may lead to an underestimation of the buffeting response and should be taken into account during the design of the bridge (e.g. [18])

Table 1. Aerodynamic derivatives KL and KM

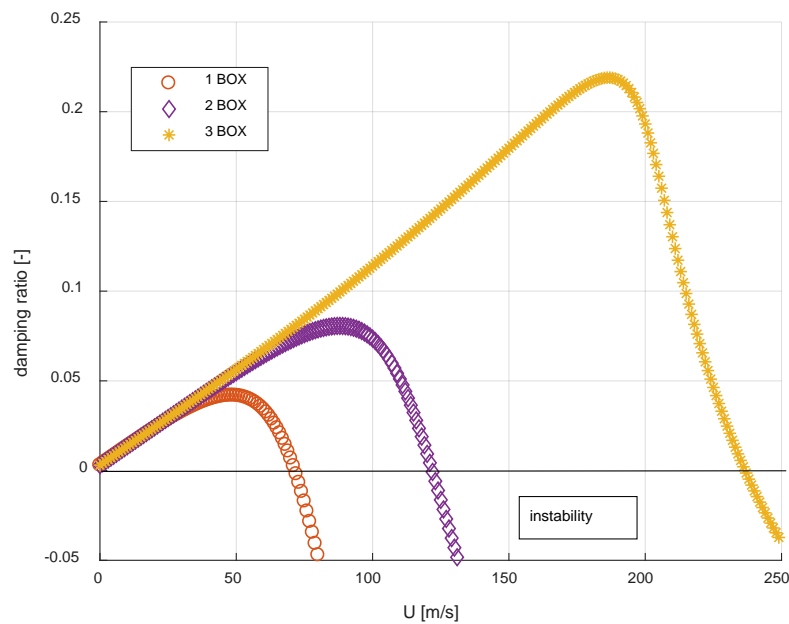| Deck	KM [1/rad]	KL [1/rad]
Storebeaelt (1 box)	1.2	4.4
Stonecuttesrs (2 boxes)	0.55	2.3
Messina (3 Boxes)	0.2	0.7

Figure 2. Stability performances of the three different cross-sections: trend of total damping ratio as a function of the mean wind speed
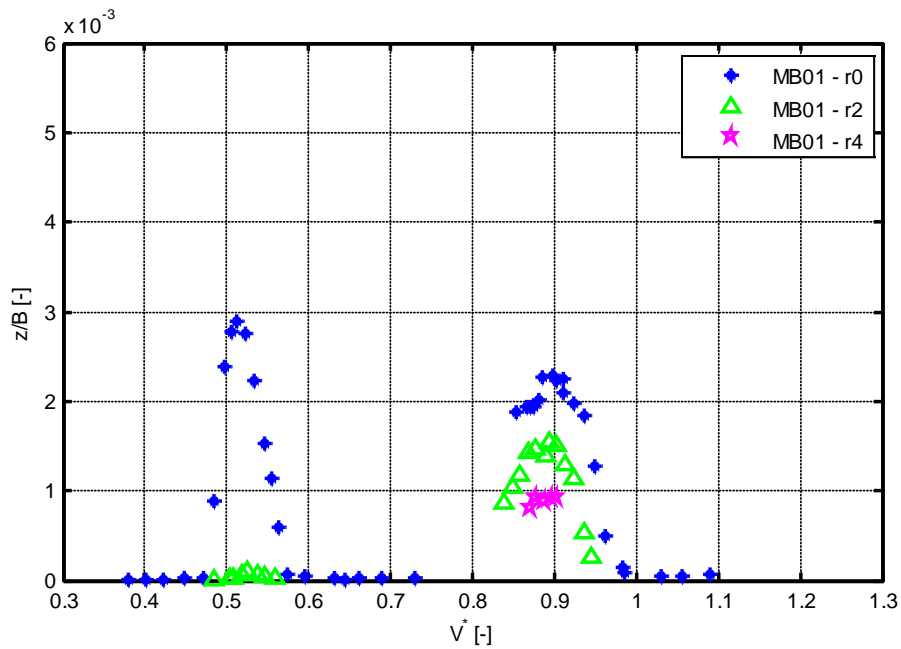
Figure 3. VIV of Messina. Steady state response: non dimensional oscillation amplitude, vertical motion as function of the reduced velocity varying the Scruton number (Sc). r0 corresponds to Sc = 0.1, r2 to Sc = 0.25, r4 to Sc = 0.44 (from [4])
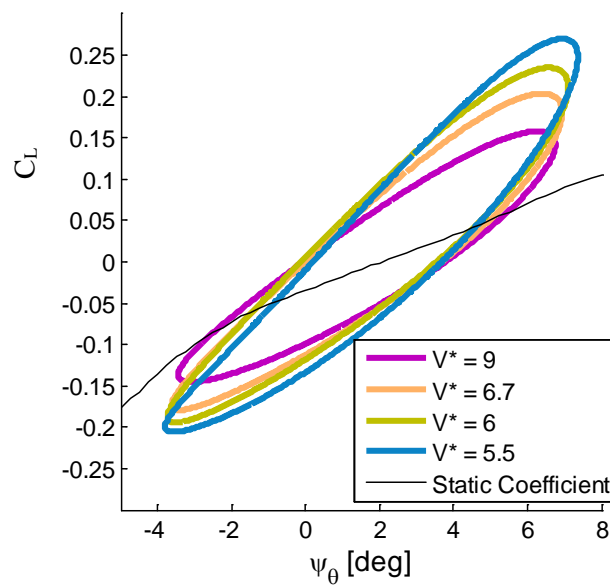

Figure 4. Nonlinear dependence of lift coefficient upon reduced velocity for large variations of the angles of attack (from -4 deg to 6 deg), from [8]

3. The HIL for the simulation of hydrodynamic forces in Wind Tunnel

At present, an experimental laboratory in which both wind and the waves effects on a floating structure can be reproduced is not available. If the numerical design of a floating bridge is required, a feasible option for its validation is to perform wind tunnel tests on a full bridge aeroelastic model, physically modelling only the part of the bridge above the water, and simulating the submerged part with a hardware in the loop (HIL) approach. This approach is currently used for floating wind turbines and could be extended to floating bridges.

3.1. The HIL approach for wind turbines

The Hardware-In-The-Loop (HIL) experimental approach allows to perform hybrid tests in which measurements, computations and actuations are performed in real time. In the specific case of the assessment of the global dynamics of a floating wind turbine through wind tunnel tests, the physical aerodynamic loads on the rotor are measured by means of a 6-components balance, which is mounted on a 2-DoF system (surge and pitch) and bears the whole wind turbine scale model (Rotor-Nacelle-Assembly and tower), see Figure 5.
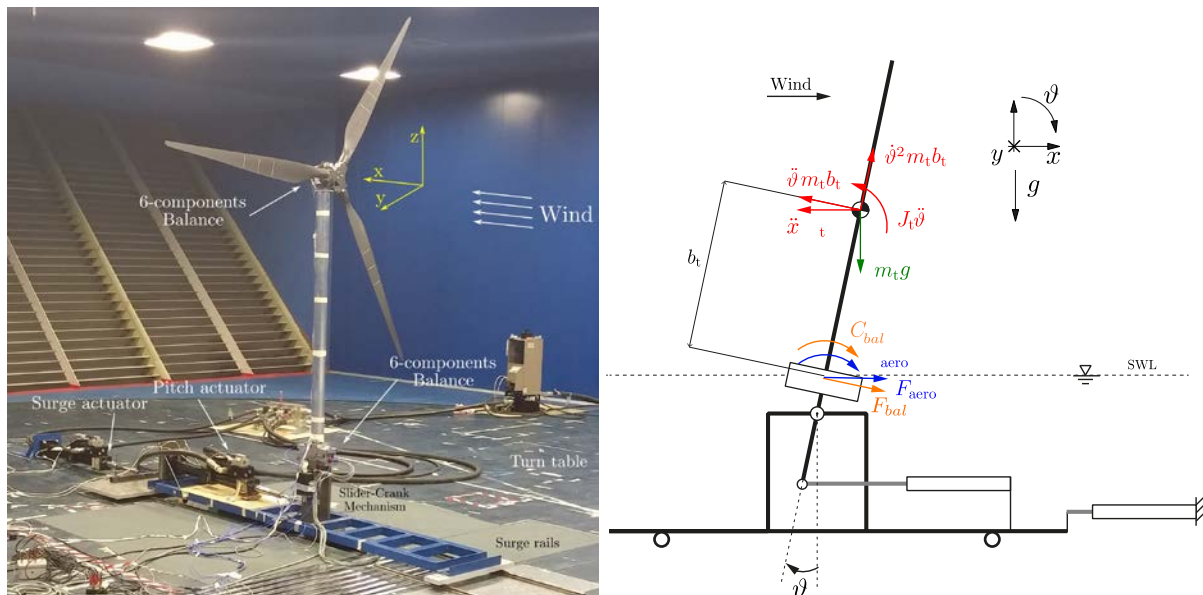

Figure 5. Picture of wind turbine model (top) and sketck of actuation and forces

The measured loads, properly conditioned, contain the aerodynamic loads which are added to computed hydrodynamic loads in order to give the physical displacements at the base of the scale model's tower to be actuated in real time. An example of control scheme is shown in Figure 7.

Both aerodynamic and hydrodynamic forces are clearly dependent on the dynamic state of the system. The combination of such forces need to be performed under specific constraints (real time) and precautions (synchronization), to obtain respectively a stable and consistent motion of the system being analyzed.

Reaching these goals within a target tolerance is possible thanks to a fast but comprehensive numerical model and an efficient real-time signal management.

3.2. Application to aeroelastic model of the bridge

The same actuation system at the base of the turbine tower could be applied at the base of the floating towers, eventually adding additional degrees of freedom. Looking at some preliminary modal simulation of the Bjørnafjorden floating bridge, obtained linearizing the hydrodynamic forces (see Master thesis

from NTNU [19]), the floating towers influence mainly the first 20 vibration modes, from 0.0125 Hz to 0.16 Hz.

　　Considering a Froude scaling for wind tunnel tests, using a geometrical scale of 1:330 for the full bridge, the frequency that should be simulated by the HIL would be between 0.2 and 3, that is in the range of operation of the actuators.

　　The expected full-scale root mean square lateral amplitude is about 2 m which in model scale would be 6 mm (so about 20 mm peak dynamic displacement), that again is in the range of the actuators. These data are consistent with the capability of the 2DoF [13] and 6DoF [14] HIL systems already available at Politecnico di Milano designed for simulating the motion of a 10MW floating wind turbine [15] with a length scale factor of 75 and a frequency scale factor of 1/25, which makes the motion of the scaled model working the sample displacement and frequency range of a possible floating bridge with the scale factors considered in the paper. For more details about the scaling procedure adopted for floating wind turbines, the reader is referred to [15]. For the sake of completeness in Table 2 surge natural frequencies of Tension Leg and Semisubmersible platform are reported on a model scale.
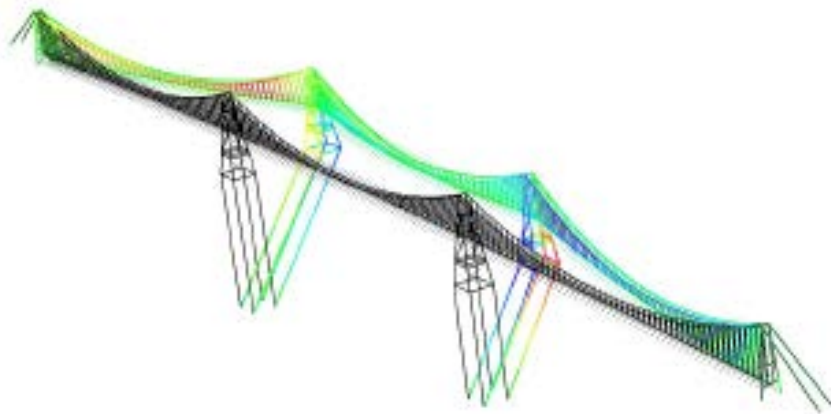

Figure 6. First vibration mode of the Bjørnafjorden floating bridge, natural frequency 0.0125 Hz, from [19]

Table 2. Frequencies of rigid modes for two platforms

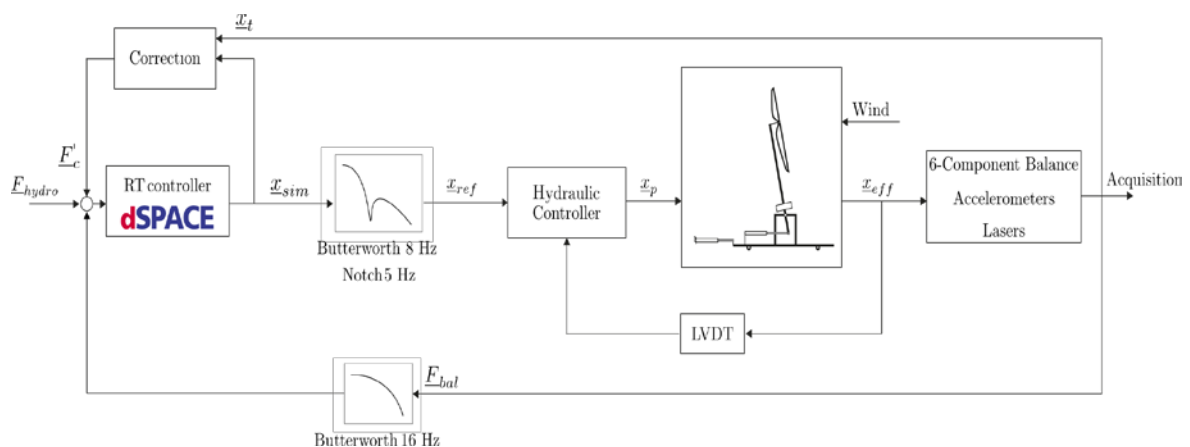| Motion	Natural frequency [Hz]
Surge (TLP)	0.75
Surge (Semisub)	0.13

Figure 7. Control scheme for HIL implementation

4. Conclusions

To cross large and deep fjords, very long bridges are being currently studied. Amongst the feasible solutions, very long spans with multi-box sections or shorter spans with floating towers are proposed in several studies.

While the multi-box technology has already been studied and it is rather well established, the floating bridge solution needs more understanding and validation. The HIL approach in wind tunnel could be an efficient tool to validate the combined effects of turbulent winds and ocean waves acting on the structure. So far it has been applied on wind turbines with success and it could be applied analogously to floating bridges.

References

[1] Larose G L and Livesey F M 1997 Performance of streamlined bridge decks in relation to the aerodynamics of a flat plate *J Wind Eng Ind Aerod* **69(Supplement C)** 851-860.

[2] Yang Y, Wu T, Ge Y, and Kareem A 2015 Aerodynamic Stabilization Mechanism of a Twin Box Girder with Various Slot Widths *Journal of Bridge Engineering* **20(3)** 04014067.

[3] Yang Y, Zhou R, Ge Y, Mohotti D and Mendis P 2015 Aerodynamic instability performance of twin box girders for long-span bridges *J Wind Eng Ind Aerod* **145**, 196-208.

[4] Belloli M, Fossati F, Giappino S and Muggiasca S 2014 Vortex induced vibrations of a bridge deck: Dynamic response and surface pressure distribution *J Wind Eng Ind Aerod* **133(Supplement C)** 160-168.

[5] Chen W L, Li H and Hu H 2014 An experimental study on the unsteady vortices and turbulent flow structures around twin-box-girder bridge deck models with different gap ratios *J Wind Eng Ind Aerod* **132** 27-36.

[6] Larsen A, Savage M, Lafrenire A, Hui M C H and Larsen, S 2008 Investigation of vortex response of a twin box bridge section at high and low Reynolds numbers *J Wind Eng Ind Aerod* **96(6-7)** 934-944.

[7] Diana G, Rocchi D and Argentini T 2013 An experimental validation of a band superposition model of the aerodynamic forces acting on multi-box deck sections. *J Wind Eng Ind Aerod* **113** 40-58

[8] Diana G, Rocchi D, Argentini T and Muggiasca S 2010 Aerodynamic instability of a bridge deck section model: Linear and nonlinear approach to force modelling *J Wind Eng Ind Aerod* **98** 363-374 B

[9] Diana G, Resta F and Rocchi D 2008 A new numerical approach to reproduce bridge aerodynamic non-linearities in time domain *J Wind Eng Ind Aerod* **96** 1871-1884

[10] Perez T and Fossen T I 2008 Joint identification of infinite-frequency added mass and fluid-memory models of marine structures *Modeling, Identification and Control* **29(3)** 93–102.

[11] Robertson A O 2017 Uncertainty analysis of OC5-DeepCwind floating semisubmersible offshore wind test campaign *The International Society of Offshore and Polar Engineers Conference*.

[12] Perez T and Fossen, T I 2009 A matlab toolbox for parametric identification of radiation-force models of ships and offshore structures *Modeling, Identification and Control* **30(1)** 1–15.

[13] Bayati I, Jonkman J, Robertson A and Platt A 2014 The effects of second-order hydrodynamics on a semisubmersible floating offshore wind turbine *Journal of Physics: Conference Series* **524(1)**.

[14] Bayati I, Gueydon S and Belloli M 2015 Study of the effect of water depth on potential flow solution of the OC4 semisubmersible floating offshore wind turbine *Energy Procedia* **80**.

[15] Ebrahimnejad L, Janoyan K D, Valentine D T and Marzocca P 2014 Investigation of the Aerodynamic Analysis of Super Long Span Bridges by Using ERA-Based Reduced-Order Models *Journal of Bridge Engineering* **19** 04014033.

[16] Argentini T, Diana G, Rocchi D and Somaschini C 2016 A case-study of double multi-modal bridge flutter: Experimental result and numerical analysis *J Wind Eng Ind Aerod* **151** 25-36

[17] Argentini T, Pagani A, Rocchi D and Zasso A 2014 Monte Carlo analysis of total damping and flutter speed of a long span bridge: Effects of structural and aerodynamic uncertainties *J Wind Eng Ind Aerod* **128** 90-104

[18] Diana G, Resta F, Rocchi D and Argentini T 2008 Aerodynamic hysteresis: wind tunnel tests and numerical implementation of a fully non linear model for the bridge aeroelastic forces *The 4th International Conference on Advances in Wind and Structures*

[19] Sondre H, Shun W G 2016 Dynamic response of suspension bridge with floating towers, *Master Thesis* Norwegian University of Science and Technology

[20] Bayati I, Belloli M, Facchinetti A 2017 Wind tunnel 2-DoF hybrid/HIL tests on the OC5 Floating Offshore Wind Turbine *36th International Conference on Ocean, Offshore and Arctic Engineering Trondheim (Norway)* OMAE2017-61763

[21] Bayati I, Belloli M, Facchinetti A Giberti H 2017 A 6DoF/HIL setup for wind tunnel hybrid tests on a 1/75 scale model of a 10 MW floating offshore wind turbine *Aimeta*

[22] Bayati I, Belloli M, Bernini L, Giberti H, Zasso A 2017 Scale model technology for floating offshore wind turbines *IET Renewable Power Generation* **11(9)** DOI:10.1049/iet-rpg.2016.0956.